

k-t FOCUSS: A General Compressed Sensing Framework for High Resolution Dynamic MRI

Hong Jung,¹ Kyunghyun Sung,² Krishna S. Nayak,² Eung Yeop Kim,³ and Jong Chul Ye^{1*}

A model-based dynamic MRI called k-t BLAST/SENSE has drawn significant attention from the MR imaging community because of its improved spatio-temporal resolution. Recently, we showed that the k-t BLAST/SENSE corresponds to the special case of a new dynamic MRI algorithm called k-t FOCUSS that is optimal from a compressed sensing perspective. The main contribution of this article is an extension of k-t FOCUSS to a more general framework with prediction and residual encoding, where the prediction provides an initial estimate and the residual encoding takes care of the remaining residual signals. Two prediction methods, RIGR and motion estimation/compensation scheme, are proposed, which significantly sparsify the residual signals. Then, using a more sophisticated random sampling pattern and optimized temporal transform, the residual signal can be effectively estimated from a very small number of k-t samples. Experimental results show that excellent reconstruction can be achieved even from severely limited k-t samples without aliasing artifacts. Magn Reson Med 61:103–116, 2009. © 2008 Wiley-Liss, Inc.

Key words: k-t BLAST/SENSE; RIGR; ME/MC; SPEAR; compressed sensing; FOCUSS

INTRODUCTION

In dynamic MRI, such as cardiac cine imaging or functional MRI, the spatio-temporal resolution is the most important quality measure. For example, in cardiac imaging, even though ultra fast imaging sequences such as balanced steady-state free precession (bSSFP) (1,2) are often used in practice, acquisition of the whole cardiac volume within a single breathhold is still a demanding task (3).

To address this issue, various reconstruction methods have been proposed using parallel coils and temporal filtering. For example, SMASH (SiMultaneous Acquisition of Spatial Harmonics) (4), GRAPPA (GeneRALized Autocalibrating Partially Parallel Acquisitions) (5), PILS

(partially parallel imaging with localized sensitivities) (6), and SENSE (SENSitivity Encoding) (7) belong to parallel imaging techniques; whereas UNFOLD (UNaliasing by Fourier-encoding the Overlaps Using the temporal Dimension) (8) uses temporal filtering to remove aliasing artifacts. However, these methods have limitations such as low signal-to-noise ratio (SNR) and the presence of aliasing artifacts for high reduction factors.

Recently, a model-based approach called k-t BLAST/SENSE has been proposed that largely overcomes the shortcomings of the aforementioned classical methods (9–12). Specifically, this approach uses a diagonal form of the signal covariance matrix obtained from training data and imposes it as a priori information for the acquisition phase. However, k-t BLAST/SENSE has a signal nulling problem at temporal DC frequency since the temporal average image is first subtracted to avoid energy concentration on temporal DC frequency in y-f space (9,13). To overcome this problem, Xu et al proposed SPEAR (SPatiotemporal domain based unaliasing employing sensitivity Encoding and Adaptive Regularization) (13) by combining k-t BLAST/SENSE and RIGR (reduced-encoding imaging by generalized-series reconstruction) (14). Unlike k-t BLAST/SENSE, SPEAR obtains the initial estimate using RIGR rather than using the temporal average. Then, the remaining aliasing artifacts are resolved by k-t BLAST/SENSE using additional lattice sampling. Consequently, SPEAR can achieve higher temporal resolution without signal nulling.

Another recent development in dynamic MRI is the introduction of the “compressed sensing (CS)” theory from the signal processing community (15,16). According to compressed sensing theory, perfect reconstruction is possible even from sampling rates dramatically smaller than the Nyquist sampling limit by solving the l_1 minimization problem, as long as the non-zero spectral signal is sparse and the samples are obtained with an incoherent basis (15). For example, k-t SPARSE (17) successfully employed the compressed sensing theory for cardiac imaging applications by transforming the time varying image using a wavelet transform along the spatial direction and Fourier transform along the temporal direction. The compressed sensing idea has been used for other applications (18,38,39).

Even though the aforementioned k-t BLAST/SENSE and the compressed sensing approach appear drastically different, a close look at the algorithms reveals striking similarity between them. We previously showed (19) that the diagonal signal covariance matrix in k-t BLAST/SENSE indeed originates from the FOCal Underdetermined System Solver (FOCUSS) (20–22) originally designed to obtain a sparse solution by successively solving quadratic optimization problems. Furthermore, they showed that the k-t BLAST/SENSE corresponds to the first iteration of so called k-t FOCUSS that is optimal from a compressed

¹Bio-Imaging & Signal Processing Lab, Department of Bio and Brain Engineering, Korea Advanced Institute of Science & Technology (KAIST), 373-1 Guseong-dong Yuseong-gu, Daejeon 305-701, Republic of Korea

²Department of Electrical Engineering, Viterbi School of Engineering, University of Southern California, EEB 406 Los Angeles, California

³Department of Radiology and Research Institute of Radiological Science, Brain Korea 21 Project for Medical Science, Yonsei University College of Medicine, Seongsanno, Seodaemun-gu, Seoul 120-752, Republic of Korea

Grant sponsor: Korea Research Foundation funded by Korean government (MOEHRD); Grant number: KRF-313-D00593

Grant sponsor: Korea Ministry of Education Science and Technology; Grant number: 2004-020-12

*Correspondence to: Jong Chul Ye, Ph.D., Department of Bio and Brain Engineering, KAIST, 373-1 Guseong-dong Yuseong-gu, Daejeon 305-701, Korea. E-mail: jong.ye@kaist.ac.kr

Received 19 July 2007; revised 28 April 2008; accepted 16 June 2008.

DOI 10.1002/mrm.21757

Published online in Wiley InterScience (www.interscience.wiley.com).

sensing perspective. The implementation of k-t FOCUSS is so simple that using only a few additional FOCUSS iterations the remaining residual aliasing artifacts of k-t BLAST/SENSE can be effectively suppressed and a high spatio-temporal resolution can be achieved (19). This suggests that k-t BLAST/SENSE indeed has a very close relation with the compressed sensing theory even though it was not revealed in the original k-t BLAST/SENSE.

The main contribution of this article is an extension of k-t FOCUSS to a novel compressed sensing framework using prediction and residual encoding, where the prediction approximately estimates the dynamic images and the residual encoding takes care of the remaining residual signals. In fact, the prediction and residual encoding framework is not new in dynamic MRI, though their importance has not been appreciated. For example, in original k-t FOCUSS (19), the temporal average corresponds to the prediction, whereas the main body of the algorithm is for the residual encoding. However, the performance of k-t FOCUSS can be further improved using better prediction since it makes the residual energy much sparser, requiring fewer k-t samples for residual encoding. This article proposes two novel prediction schemes. First, similar to SPEAR, a RIGR-based prediction scheme is proposed. The novelty here is to exploit additional temporal correlation along the read-out direction to further improve the prediction efficiency of the conventional RIGR. Second, a motion estimation/compensation (ME/MC) approach is proposed that exploits the correlation between the frames using motion vectors similar to video coding. Both methods significantly sparsify the residual signal compared with the temporal average. Furthermore, using more sophisticated random sampling pattern and an optimized temporal transform, the residual signal can be effectively estimated with a very small number of k-t samples.

THEORY

Compressed Sensing

Consider the Cartesian trajectory. The readout direction is along the k_x axis, and k_y denotes the phase encoding direction. The samples along the readout direction are fully sampled within TR. Let $\sigma(y, t)$ denote the unknown image content (for example, proton density, T1/T2 weighted image, etc.) on y at time instance t . Then, the k-space measurement $v(k, t)$ at time t is given by

$$v(k, t) = \int \sigma(y, t) e^{-j2\pi ky} dy, \quad [1]$$

or in a vector form:

$$\mathbf{v} = \mathbf{F}_y \boldsymbol{\sigma} \quad [2]$$

where \mathbf{F}_y denotes the Fourier transform along the y -direction, and \mathbf{v} and $\boldsymbol{\sigma}$ denote the stacked k-t space measurement vectors and the discretized image content to be reconstructed, respectively. For high acceleration, the length of the k-t measurement vector \mathbf{v} is much smaller than that of $\boldsymbol{\sigma}$, resulting in a highly underdetermined inverse problem.

In cardiac cine imaging, the signal $\sigma(y, t)$ can be effectively sparsified using Fourier transform along the temporal

direction due to the periodic motion of the heart. More specifically, let $\rho(y, f)$ denote the 2-D spectral signal in the y - f domain. Then, we have the following 2-D Fourier relationship:

$$v(k, t) = \iint \rho(y, f) e^{-j2\pi(ky+ft)} dy df, \quad [3]$$

or in a vector form:

$$\mathbf{v} = \mathbf{F}_y \mathbf{F}_t \boldsymbol{\rho} \quad [4]$$

where \mathbf{F}_t denotes the Fourier transform along the t -direction. Then, the sparsity of the unknown signal can be exploited by solving the following l_1 minimization problem (15,16):

$$\begin{aligned} & \text{minimize} && \|\boldsymbol{\rho}\|_1 \\ & \text{subject to} && \|\mathbf{v} - \mathbf{F}_y \mathbf{F}_t \boldsymbol{\rho}\|_2 \leq \epsilon \end{aligned} \quad [5]$$

where $\|\cdot\|_1$ and $\|\cdot\|_2$ denote the l_1 and l_2 norm, respectively, and ϵ denotes the noise level.

k-t FOCUSS with Prediction/Residual Encoding

k-t FOCUSS was developed to address the l_1 minimization problem (Eq. [5]) using a reweighted quadratic optimization technique (19). This article extends the original formulation in Ref. 19 to a more general prediction/residual encoding framework. More specifically, the unknown signal $\boldsymbol{\rho}$ is decomposed into the predicted signal $\boldsymbol{\rho}_0$ and the residual signal $\Delta\boldsymbol{\rho}$:

$$\boldsymbol{\rho} = \boldsymbol{\rho}_0 + \Delta\boldsymbol{\rho}. \quad [6]$$

Our goal is now to try to impose the sparsity on the residual signal $\Delta\boldsymbol{\rho}$ rather than the total signal $\boldsymbol{\rho}$. Specifically, the compressed sensing approach for a dynamic MR image can be represented as follows:

$$\begin{aligned} & \text{minimize} && \|\Delta\boldsymbol{\rho}\|_1 \\ & \text{subject to} && \|\mathbf{v} - \mathbf{F}_y \boldsymbol{\rho}_0 - \mathbf{F} \Delta\boldsymbol{\rho}\|_2 \leq \epsilon \end{aligned} \quad [7]$$

where $\mathbf{F} = \mathbf{F}_y \mathbf{F}_t$. Algorithm 1 describes the pseudo-code implementation of k-t FOCUSS, which solves Eq. [7] using reweighted quadratic optimization.¹ To reduce the total number of required k-t samples, we need a high-performance prediction scheme to make the residual signal $\Delta\boldsymbol{\rho}$ as sparse as possible. However, better prediction often requires additional k-t samples. This illustrates the fundamental trade-off between prediction and residual encoding, which should be carefully studied for best performance.

Such trade-off between prediction/residual encoding has an important parallel in video compression such as MPEG (Motion Picture Expert Group) (23), which exploits temporal redundancies to compress the video. A simplified coding structure of MPEG without bidirectional (**B**) picture is constituted in Fig. 1a. There are two types of frame coding. First, the intra pictures (**I**) are obtained using discrete

¹Note that k-t FOCUSS solves the l_1 minimization problem by setting $p = 0.5$ in Eq. [10] (19).

Algorithm 1 Pseudo-code implementation of k-t FOCUSS

1. Initialize the weighting matrix \mathbf{W}_0 .
2. Calculate the predicted signal ρ_0 .
3. For each $l = 0, 1, \dots$, repeat following until converged.

- a. Solve the following l_2 optimization problem for \mathbf{q}_l :

$$\min \|\mathbf{q}_l\|_2, \quad \text{subject to } \|\mathbf{v} - \mathbf{F}\rho_0 - \mathbf{F}\mathbf{W}_l\mathbf{q}_l\|_2 \leq \epsilon \quad [8]$$

- b. Calculate ρ_{l+1} :

$$\begin{aligned} \rho_{l+1} &= \rho_0 + \mathbf{W}_l\mathbf{q}_l \\ &= \rho_0 + \Theta_l\mathbf{F}^H(\mathbf{F}\Theta_l\mathbf{F}^H + \lambda\mathbf{I})^{-1}(\mathbf{v} - \mathbf{F}\rho_0), \quad \text{where } \Theta_l = \mathbf{W}_l\mathbf{W}_l^H. \end{aligned} \quad [9]$$

- c. update \mathbf{W}_{l+1} :

$$\mathbf{W}_{l+1} = \begin{pmatrix} |\Delta\rho_{l+1}(1)|^p & 0 & \dots & 0 \\ 0 & |\Delta\rho_{l+1}(2)|^p & \dots & 0 \\ \vdots & \vdots & \ddots & \vdots \\ 0 & 0 & \dots & |\Delta\rho_{l+1}(N)|^p \end{pmatrix}, \quad 1/2 \leq p \leq 1 \quad [10]$$

- d. increase l , and go to the step (a).

cosine transform (DCT) by exploiting the spatial correlation as done in still image compression (23). Then, the predicted pictures (\mathbf{P}) are coded using past reference frames and previously predicted pictures. The \mathbf{P} frame can compress the data significantly by exploiting the temporal redundancies using motion estimation and compensation (ME/MC). The remaining residual signals that cannot be estimated from ME/MC are then encoded using residual encoding with DCT. Now, we can observe the fundamental trade-off in video coding. As the reference \mathbf{I} frame becomes more accurate and the motion estimation accuracy increases using very dense motion vector fields, the residual signal can be significantly sparsified. But, such accurate \mathbf{I} frame and dense motion fields will introduce additional coding bits. On the contrary, if a smaller number of bits is used for prediction, the residual signal becomes large, requiring significant number of bits for residual coding. Therefore, the optimal bit allocation for \mathbf{I} frame coding, motion vectors, and residual coding has been an important issue in video compression (23).

This article presents two prediction/residual encoding schemes. The first is based on the 2-D RIGR method and the latter uses ME/MC. Both methods are effective in sparsifying the residual signal. Moreover, our k-t FOCUSS framework is so general that other types of high performance prediction/residual encoding could be employed to achieve the high performance.

IMPLEMENTATION OF PREDICTION/RESIDUAL ENCODING

Recall that the $(l + 1)$ -th update of the k-t FOCUSS framework can be summarized as follows:

$$\rho_{l+1} = \underbrace{\rho_0}_{\text{prediction}} + \underbrace{\Theta_l\mathbf{F}^H(\mathbf{F}\Theta_l\mathbf{F}^H + \lambda\mathbf{I})^{-1}(\mathbf{v} - \mathbf{F}\rho_0)}_{\text{residual encoding}}, \quad [11]$$

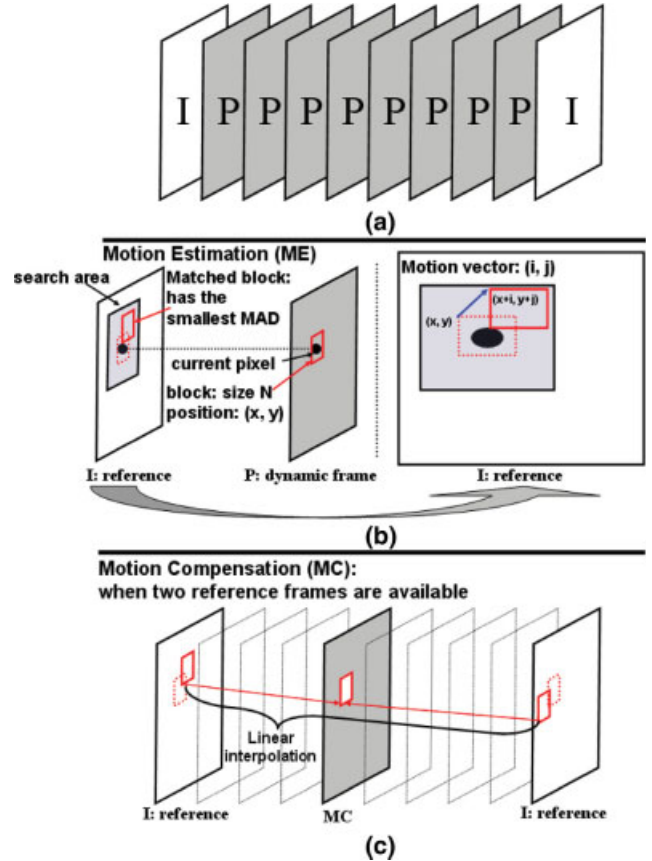


FIG. 1. The proposed methods utilize ideas from video compression and the MPEG standard. (a) MPEG video with I and P frames. (b) Motion estimation, and (c) motion compensation used in k-t FOCUSS MAD implies mean absolute difference. [Color figure can be viewed in the online issue, which is available at www.interscience.wiley.com.]

where $\Theta_l = \mathbf{W}_l \mathbf{W}_l^H$. This section explains how to optimize the prediction and residual encoding to improve the reconstruction quality of the k-t FOCUSS.

Prediction Step

Prediction by 2-D RIGR

The main assumption of RIGR is that in most dynamic imaging problems, the high resolution image content does not change drastically from one image to another and therefore need not be obtained every time (14). As shown in Fig. 2, the sampling pattern for RIGR includes fully sampled high resolution references and the additional dynamic encoding for the low frequency region of k-t space. Then, spatial basis functions of a generalized series model are constructed from the reference image, and dynamic images are estimated using spatial basis functions of the generalized series model and fully sampled low frequency data. Even though this RIGR estimate is not perfect in describing sophisticated temporal variations in dynamic MRI, it can be a good prediction that sparsifies residual signal significantly as shown in SPEAR (13).

However, as shown in Fig. 3(a), the original RIGR does not exploit the temporal correlation between the neighboring pixels along the read-out direction. Considering the parallel in video coding, better prediction can be obtained by exploiting the temporal correlation between the frames along the read-out as well as the phase encoding direction as shown in Fig. 3(b). More specifically, when two reference images are obtained, let $\Delta\rho_{\text{ref}}(x, y)$ be the difference image obtained by subtracting the first reference image from the second at (x, y) . Then, the n -th basis function for the generalized series model is given by

$$\phi_n(x, y) = |\Delta\rho_{\text{ref}}(x, y)| e^{i2\pi n \Delta k y}, \quad [12]$$

where $\Delta k = 1/\text{FOV}$. When only one reference frame is measured, we can simply set $\Delta\rho_{\text{ref}}(x, y)$ with the only reference itself without difference from some other frames. In

our 2-D RIGR, the difference image $\Delta\rho(x, y; t)$ is estimated using the following 2-D expansion:

$$\Delta\rho(x, y; t) = \sum_{k=-P/2}^{P/2} \sum_{n=-M/2}^{M/2-1} c_x(k, n; t) \phi_n(x - k, y), \quad [13]$$

where P and M are the number of neighboring pixels along the read-out direction, and phase encoding direction respectively, and $\{c_x(k, n; t)\}_{n=-M/2}^{M/2-1}$ now becomes a two dimensional filter, which is dependent on the read-out coordinate x . Note that in the conventional RIGR, $P = 0$ and the filter is one dimensional.

To use Eq. [13], we must determine the coefficients $c_x(k, n; t)$. If both sides of Eq. [13] are Fourier transformed along the phase encoding direction, we have:

$$\Delta d(x, m, t) = \sum_{k=-P/2}^{P/2} \sum_{n=-M/2}^{M/2-1} c_x(k, n; t) \Delta d_{\text{ref}}(x - k, m - n), \quad [14]$$

where $\Delta d(x, m, t)$ and $\Delta d_{\text{ref}}(x, m)$ represent the 1-D Fourier transform of $\Delta\rho(x, y, t)$ and $|\Delta\rho_{\text{ref}}(x, y)|$ along the phase encoding direction y , respectively. Here, $\Delta d(x, m, t)$ can be obtained from the fully sampled center region in the RIGR sampling pattern. Then, we have:

$$\mathbf{H} \mathbf{c}_x(t) = \mathbf{d}_x(t), \quad [15]$$

where

$$\begin{aligned} \mathbf{d}_x(t) &= [\Delta d(x, -M/2, t) \quad \Delta d(x, -M/2 + 1, t) \cdots \\ &\quad d(x, M/2 - 1, t)]^T \in \mathbb{C}^M \\ \mathbf{c}_x(t) &= [c_x(-P/2, -M/2, t) \quad c_x(-P/2 + 1, -M/2, t) \cdots \\ &\quad c_x(P/2, M/2 - 1, t)]^T \in \mathbb{C}^{(P+1)M} \end{aligned} \quad [16]$$

and

$$\mathbf{H} = \begin{bmatrix} \Delta d_{\text{ref}}(x + P/2, 0) & \Delta d_{\text{ref}}(x + P/2 - 1, 0) & \cdots & \Delta d_{\text{ref}}(x - P/2, -M + 1) \\ \Delta d_{\text{ref}}(x + P/2, 1) & \Delta d_{\text{ref}}(x + P/2 - 1, 1) & \cdots & \Delta d_{\text{ref}}(x - P/2, -M + 2) \\ \vdots & \vdots & \ddots & \vdots \\ \Delta d_{\text{ref}}(x + P/2, M - 1) & \Delta d_{\text{ref}}(x + P/2 - 1, M - 1) & \cdots & \Delta d_{\text{ref}}(x - P/2, 0) \end{bmatrix} \in \mathbb{C}^{M \times (P+1)M}. \quad [17]$$

Hence, $\mathbf{c}_x(t)$ can be calculated as follows:

$$\mathbf{c}_x(t) = \mathbf{H}^H (\mathbf{H} \mathbf{H}^H)^{-1} \mathbf{d}_x(t). \quad [18]$$

Prediction by ME/MC

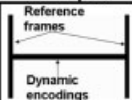
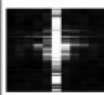

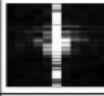

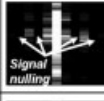
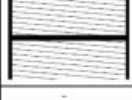
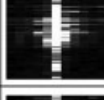
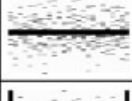
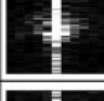

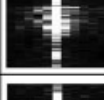

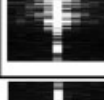
Motion estimation and compensation (ME/MC) is an essential step in video coding that uses motion vectors to exploit the temporal redundancies between frames (23). To discuss how we can apply ME/MC to dynamic MRI, we will first review each process. ME is a process for the estimation of motion vectors, and the most popular method used in video coding is the Block Matching Algorithm (BMA). Suppose that \mathbf{B}_m indicates a block, then the following

relation should be satisfied (24):

$$\bigcup_{m \in \mathbf{M}} \mathbf{B}_m = \Lambda, \quad \mathbf{B}_m \cap \mathbf{B}_n = \emptyset, \quad \text{when } m \neq n. \quad [19]$$

Here, \mathbf{M} is a set of the indexes of blocks and Λ implies the set of all of the pixels in the one image. The block matching algorithm calculates the mean absolute difference (MAD) between the reference frame σ_{ref} and the current frame σ_{cur} over each block \mathbf{B}_m in order to obtain a motion vector \mathbf{d}_m by minimizing the following cost function:

$$\mathbf{E}(\mathbf{d}_m) = \sum_{\mathbf{x} \in \mathbf{B}_m} |\sigma_{\text{ref}}(\mathbf{x} + \mathbf{d}_m) - \sigma_{\text{cur}}(\mathbf{x}, t)|. \quad [20]$$

Sampling pattern on k-t space	Properties	Reconstructed y-f signal
	<ul style="list-style-type: none"> ● RIGR [14] <ul style="list-style-type: none"> - Fully sampled PEs in center region + fully sampled reference frames at the beginning and the end of the dynamic frames. - 1-D filter is used. 	
	<ul style="list-style-type: none"> ● 2-D RIGR <ul style="list-style-type: none"> - The same sampling pattern as in the RIGR. - Exploits the correlation along read-out direction. 	
	<ul style="list-style-type: none"> ● k-t BLAST/SENSE [9] <ul style="list-style-type: none"> - Fully sampled PEs in center region + sheared lattice pattern. - Initialization with temporal average. - Signal nulling problem appears in y-f space. 	
	<ul style="list-style-type: none"> ● SPEAR [13] <ul style="list-style-type: none"> - Similar lattice sampling pattern used for k-t BLAST/SENSE + fully sampled reference frames at the beginning and the end of the dynamic frames. - Initialization with RIGR. 	
	<ul style="list-style-type: none"> ● k-t FOCUSS with temporal average [19] <ul style="list-style-type: none"> - Fully sampled PEs in center region + randomly sampled high frequency data. - Initialization with temporal average. 	
	<ul style="list-style-type: none"> ● k-t FOCUSS with 2-D RIGR <ul style="list-style-type: none"> - The same sampling pattern as original k-t FOCUSS + additional two fully sampled reference frames. - Initialization with 2-D RIGR. 	
	<ul style="list-style-type: none"> ● k-t FOCUSS with ME/MC <ul style="list-style-type: none"> - The same sampling pattern as k-t FOCUSS with 2-D RIGR. - Initialization with the motion compensated frames. 	

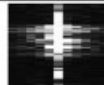


FIG. 2. Summary of various dynamic MRI techniques.

In Eq. [20], the most robust method is to find the vector with the smallest MAD within a search window, as shown in Fig. 1b. Now, MC can be addressed to decode the predicted frames using the motion vectors obtained during ME. In contrast to the ME process, MC is a quite simple process since it just relocates pixels or blocks on the reference frames according to the corresponding motion vectors.

More specifically, if the motion vector for the (x, y, t) coordinate is $[i, j]$, the corresponding pixel values on the motion compensated frame σ_{mc} can be copied from the reference frame σ_{ref} as follows:

$$\sigma_{mc}(x, y, t) = \sigma_{ref}(x + i, y + j). \quad [21]$$

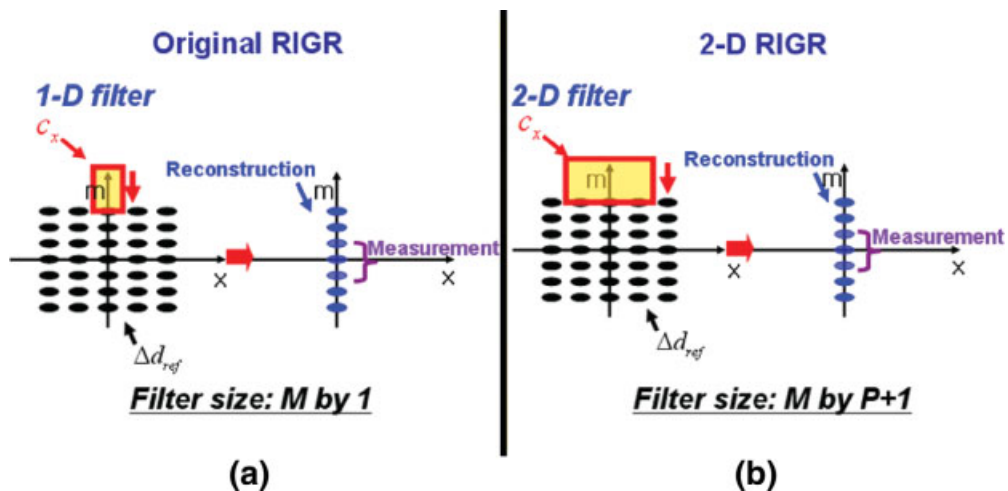


FIG. 3. Prediction scheme for (a) RIGR with the 1-D filter. By expanding filter dimension to the read-out direction as shown in (b), the spatial correlation along the read-out direction can be effectively exploited. [Color figure can be viewed in the online issue, which is available at www.interscience.wiley.com.]

To employ ME/MC within dynamic MRI, there are several technical issues to address. First, at least one reference frame σ_{ref} is required in Eq. [20]. This issue can be easily resolved since RIGR has already employed the reference frames as discussed in the previous section. These reference frames can fulfill the same role as **I** frames in MPEG coding and can be used in the MC step. The main technical difficulty, however, comes from the existence of the current frame σ_{cur} of Eq. [20]. Unlike the encoder in the video coding, the current frame σ_{cur} is not available in a highly accelerated dynamic MRI since the only available data in the highly accelerated dynamic MRI is the reduced number of k-space data. Does this imply that the ME process is not feasible? Fortunately, this issue can be addressed using an additional reconstruction step before the ME/MC. More specifically, suppose there exists a reconstruction algorithm that can reconstruct the current frame approximately. Now, let $\hat{\sigma}_{\text{cur}}$ be the estimated current frame. Then, the cost function for the ME in Eq. [20] can be modified as following:

$$\mathbf{E}(\mathbf{d}_m) = \sum_{\mathbf{x} \in \mathbf{B}_m} |\sigma_{\text{ref}}(\mathbf{x} + \mathbf{d}_m) - \hat{\sigma}_{\text{cur}}(\mathbf{x}, t)|, \quad [22]$$

where the estimated current frame $\hat{\sigma}_{\text{cur}}$ is used for the ME. Of course, a better reconstruction algorithm can provide accurate estimation of the current frame $\hat{\sigma}_{\text{cur}}$ and more consistent motion vectors accordingly. We found that our k-t FOCUSS in Ref. 19 can work toward such a goal. With the resulting motion vectors, the MC step can be easily implemented using Eq. [21].

Although our ME step is more involved than its counterpart in video coding, our ME process offers many advantages. In video coding, an encoder transmits the motion vectors separately using additional bits. This implies that a dense motion vector field is usually prohibited. In contrast, the motion vectors are estimated from the data itself in a dynamic MR without additional sample allocation. Therefore, a dense motion vector field as well as multiple reference frames can be used in the ME step to improve the estimation performance. For example, when there are two reference frames, Eq. [21] can be modified using linear interpolation as illustrated in Fig. 1c. More specifically, suppose that two reference frames are measured at times 0 and T , and the motion vectors for a certain pixel or block positioned on (x, y, t) with respect to each reference frame are (i_1, j_1) and (i_2, j_2) , respectively. Then, the interpolated MC is as follows.

$$\sigma_0(x, y, t) = \frac{t\sigma_{\text{ref1}}(x_1, y_1) + (T - t)\sigma_{\text{ref2}}(x_2, y_2)}{T} \quad [23]$$

where $x_1 = x + i_1$, $y_1 = y + j_1$ and $x_2 = x + i_2$, $y_2 = y + j_2$, and where σ_{ref1} and σ_{ref2} represent the measured reference frames at times 0 and T .

Second, since no additional information is required with more sophisticated ME/MC, a modified block-based ME/MC with overlapping blocks can be implemented to remove the blocking artifact. Here, the block size is fixed to 2 pixels \times 2 pixels, and the total number of obtained motion vectors is equal to the number of total pixels on the image due to the nature of overlapping block-based ME/MC. This

overlapping ME/MC procedure with small block size can effectively remove the blocking artifacts through averaging.

There are many advantages to using ME/MC to obtain the predicted signal ρ_0 . First, finer dynamic image structure can be obtained without noticeable blurring because MC just relocates the corresponding pixels of the fully sampled reference frames. Second, unlike the RIGR, k-t samples are not fully allocated for the prediction step because the estimation is performed on the image domain rather than the frequency domain. Therefore, most of the k-t samples can be reused in the following residual encoding step. Third, the algorithm can be applied to any k-t space trajectory including spiral or radial, since all the ME/MC steps are done in the image domain. In contrast, the RIGR algorithm is specifically tailored to the Cartesian trajectory.

Residual Encoding

The main focus of the residual encoding step is to efficiently estimate the residual signal using a small number of k-t samples. Since the prediction step provides a sparse residual, k-t FOCUSS can effectively exploit the sparsity of the residual signal. However, even for a given prediction scheme, it is still possible to further optimize the residual encoding.

In general, the temporal transform \mathbf{F}_t in Eq. [4] is not necessarily a Fourier transform. In dynamic imaging such as cardiac cine, a Fourier transform along the temporal direction effectively sparsifies the signal due to the periodic nature of cardiac motion. However, for nonperiodic motion like fMRI, we can often get a significantly sparser signal from a Karhunen-Loeve Transform (KLT) as compared to a Fourier transform (19) since the KLT represents motions of images with only a few coefficients corresponding to some significant eigenvectors. In order to calculate the eigenvectors for the KLT, the covariance matrix for the temporal variation of the image content $\sigma(x, t)$ is calculated using the densely sampled low frequency region of the k-t samples.

So far, the temporal transform has been discussed as a sparsifying transform. Another option remains, which is the spatial transform \mathbf{F}_y . For example, k-t SPARSE (17) employs a wavelet transform on the spatial domain and a Fourier transform along the temporal direction to make the signal sparse. The wavelet transform converts spatial information into a low-frequency approximate image and high-frequency detail components. Recall that high-frequency detail components tend to be sparse thanks to the property of wavelets, which may be exploited to reduce the k-t samples. However, careful consideration is required in using wavelet transform on the spatial domain. Depending on the regularity of the wavelets, the reconstructed image could be a little blurred or exhibit cartoon-like artifacts even though aliasing artifacts can be effectively removed.

METHOD

Downsampling Experiments

We acquired two sets of cardiac cine from different volunteers using a 1.5 T Philips scanner at Yonsei University Medical Center, Seoul, Korea. Each of sets is composed of 25 frames of full k-space data. The field of view (FOV) of the first and second data set were $345.00 \times 270.00 \text{ mm}^2$

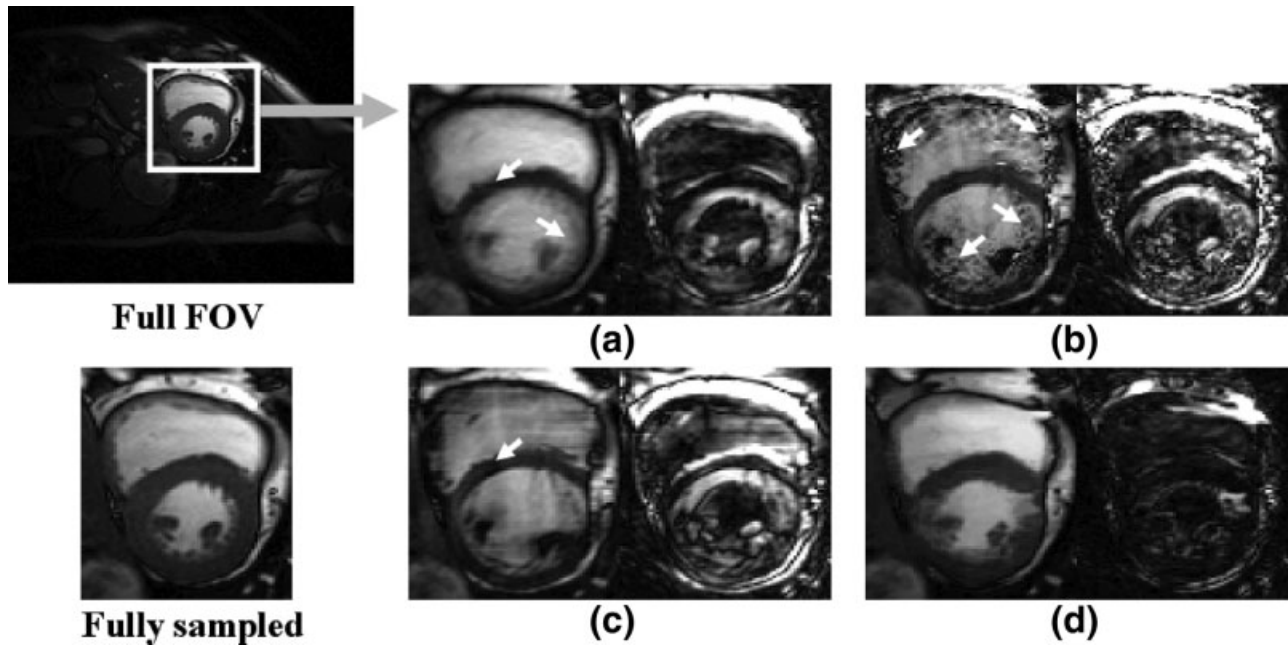


FIG. 4. Comparison of various prediction schemes. Temporal average, conventional RIGR, 2-D RIGR, and ME/MC are shown in (a), (b), (c), and (d), respectively. To compare these clearly, the difference images are also illustrated. (a), (b), and (c) do not follow the true motion. In fully sampled image, systole cardiac phase is shown, but the cardiac boundary of (a), (b), and (c) still remain in diastole phase (indicated with white arrow). Furthermore, (b) is severely degraded because spatial correlation cannot be fully exploited in the conventional RIGR. In contrast, the degraded structure can be recovered better in (c). Finally, (d) shows greatly improved prediction result, which is very close to the fully sampled image.

and $306.00 \times 260.00 \text{ mm}^2$, respectively. The matrix size for both scanning was 220×256 , which corresponds to 220 phase encoding steps and 256 samples in frequency encoding. In these experiments, the phase encoding direction is vertical. The slice thickness was 10.0 mm, and the acquisition sequence was balanced steady-state free precession (bSSFP) with a flip angle of 50° in both data acquisition. The heart rate of the first and the second subject were 75 bpm and 65 bpm, respectively, and the retrospective cardiac gating was used for each acquisition. The repetition time TR was 3.17 ms and 3.23 ms, respectively.

In Vivo Experiments

In vivo experiments were performed on a GE Signa EXCITE 3.0T system (General Electric Healthcare, Waukesha, WI) at the University of Southern California, Los Angeles, with gradients capable of 40 mT/m amplitude and a 150 T/m/s slew rate. A body coil was used for RF transmission and an 8-channel phased array cardiac coil was used for signal reception. The transmit gain was calibrated using a standard pre-scan and the center frequency was adjusted over a 3D region of interest containing the left ventricle (LV). Synchronization with the cardiac cycle was achieved with prospective triggering based on a plethysmograph signal. The Institutional Review Board of the University of Southern California approved the imaging protocols. Each subject was screened for magnetic resonance imaging risk factors and provided informed consent in accordance with institutional policy.

The acquisition sequence was balanced SSFP, and imaging parameters were as follows: TR = 3.7 ms, flip angle

= 45° , slice thickness = 5 mm, FOV = 30 cm, views per segment = 10, cardiac phase = 25, and matrix size = 240×256 (full k-space data).

According to Bieri et al. (25), in balanced SSFP, random sampling introduces significant transient artifacts that are related to unbalanced phase due to eddy currents stemming from the phase encoding gradient. These effects are accentuated when there are large jumps in the phase encode order. This observation may incur some concerns about the applicability of k-t FOCUSS for cardiac cine imaging. Recall that the main requirement of compressed sensing is the incoherent measurement bases (16). Random k-t sampling is one sampling pattern which can satisfy such a requirement, but is not the only sampling pattern. As long as we can find other sampling patterns to make the measurement bases incoherent, we can use them for k-t FOCUSS. Interestingly, Bieri et al. (25) proposed a simple and effective eddy current compensation method for bSSFP by pairing the consecutive PE steps.

Hence, for the accelerated acquisition, we employed the pair-wise random sampling pattern described in Fig. 8a. More specifically, the fully sampled eight lowest spatial frequencies were acquired and 32 additional random samples were obtained by pairing the consecutive PE steps. Consequently, the total number of phase encoding steps was 40 and the acceleration factor was six.

RESULTS

Downsampling Experiments

We have compared k-t FOCUSS results with k-t BLAST/SENSE and SPEAR. For the k-t BLAST/SENSE and SPEAR,

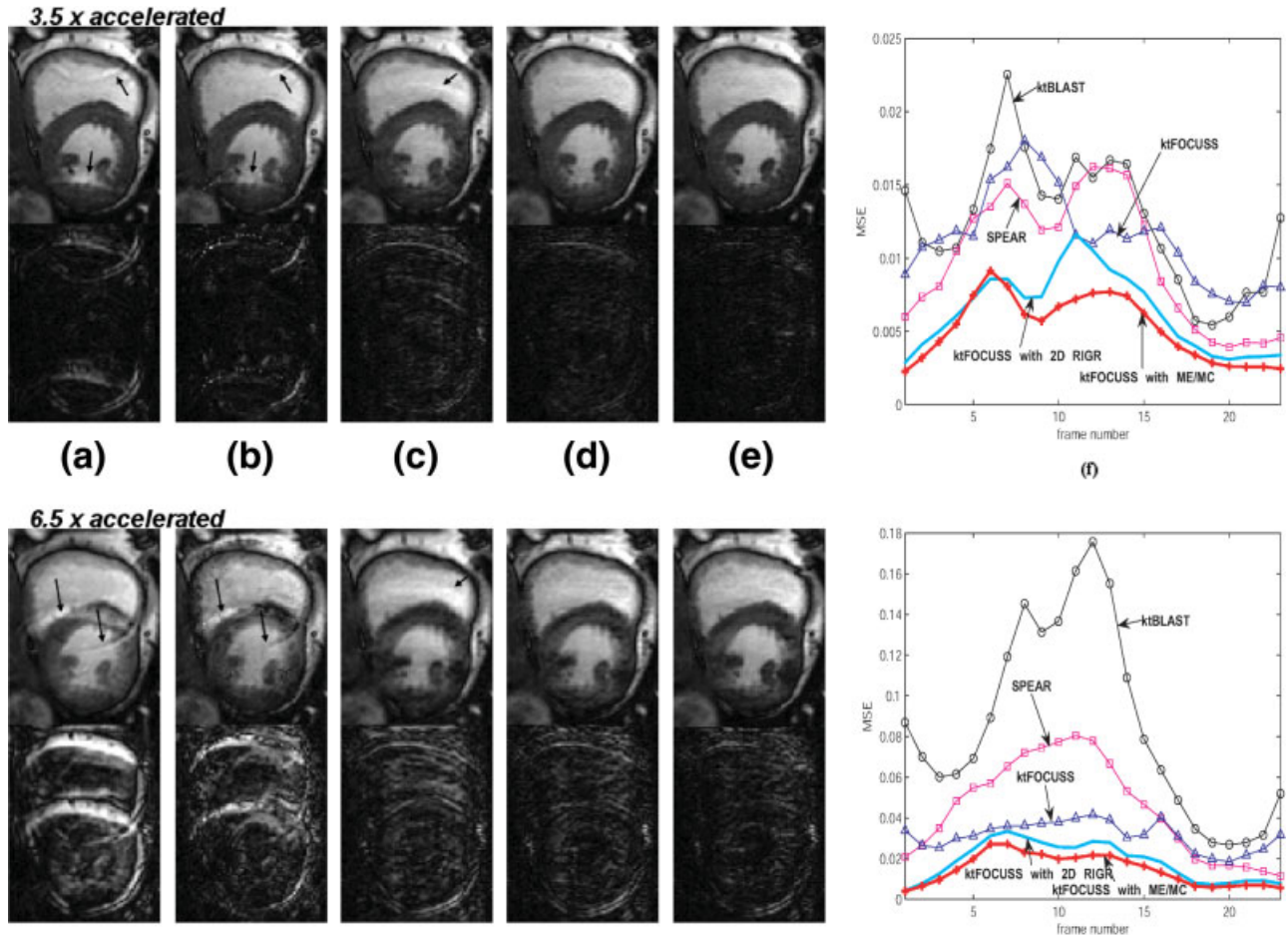


FIG. 5. Comparison of various reconstruction methods, (a) k-t BLAST, (b) SPEAR, (c) k-t FOCUSS with temporal average, (d) k-t FOCUSS with 2-D RIGR, and (e) k-t FOCUSS with ME/MC. (f) The frame-by-frame MSE plot for each method. The top row shows the reconstructed results at the 3.5 fold acceleration. All of the results show quite good quality, but (a), (b), and (c) show remaining aliasing artifacts (indicated by black arrows). The bottom row shows the results at the 6.5 fold acceleration. The aliasing artifacts become noticeable. The aliasing artifacts are indicated by black arrows.

the lattice sampling patterns as shown in Fig. 2 were employed. For k-t FOCUSS implementation, the random sampling patterns in Fig. 2 were used. As discussed in Ref. 19, a random sampling pattern using Gaussian distribution outperforms uniform sampling. In these simulations, fully sampled low frequency regions composed of the eight lowest spatial frequencies are included to provide initial low resolution images \mathbf{W}_0 .

To verify the prediction and residual encoding concept in k-t FOCUSS, we first compared the performance of various prediction schemes. Figure 4 shows the various predictions for the first data set. Among these, ME/MC based prediction provides the best visual reconstruction quality. And, 2-D RIGR outperforms the conventional RIGR.

Now, we compared the k-t FOCUSS with k-t BLAST/SENSE and SPEAR at the reduction factor of 3.5 and 6.5 in Fig. 5. For the 3.5-fold acceleration, fully sampled 8 phase encoding lines in the low frequency region and 53 phase encodings for the high frequency region out of a total of 220 phase encodings were sampled. In a similar way, for the 6.5-fold acceleration, fully sampled 8 phase encoding lines in the low frequency region and

26 phase encodings for the high frequency region were sampled. The reconstruction results of k-t BLAST/SENSE, SPEAR, k-t FOCUSS with temporal average, k-t FOCUSS with 2-D RIGR, and k-t FOCUSS with ME/MC are illustrated in Fig. 5a–e, respectively along with the difference images in order to clearly show the improvement. The figures in the top row illustrate the results for the 3.5-fold acceleration. In this case, all of the results show clear structures of heart while different pattern of aliasing artifacts are observed especially in k-t BLAST/SENSE, SPEAR and k-t FOCUSS with temporal average. When k-t FOCUSS with 2-D RIGR or k-t FOCUSS with ME/MC is used, the aliasing artifacts are clearly removed and only small residual error remains on cardiac boundary. For the quantitative comparison, we plotted the frame-by-frame Mean Squared Error (MSE) in Fig. 5f. Although k-t BLAST/SENSE, SPEAR, and k-t FOCUSS with temporal average do not show big difference, k-t FOCUSS with 2-D RIGR and ME/MC clearly reduce MSE over all frames. Similar experiments were performed for the 6.5-fold down sampled data and the results are shown in the bottom row of Fig. 5. Here,

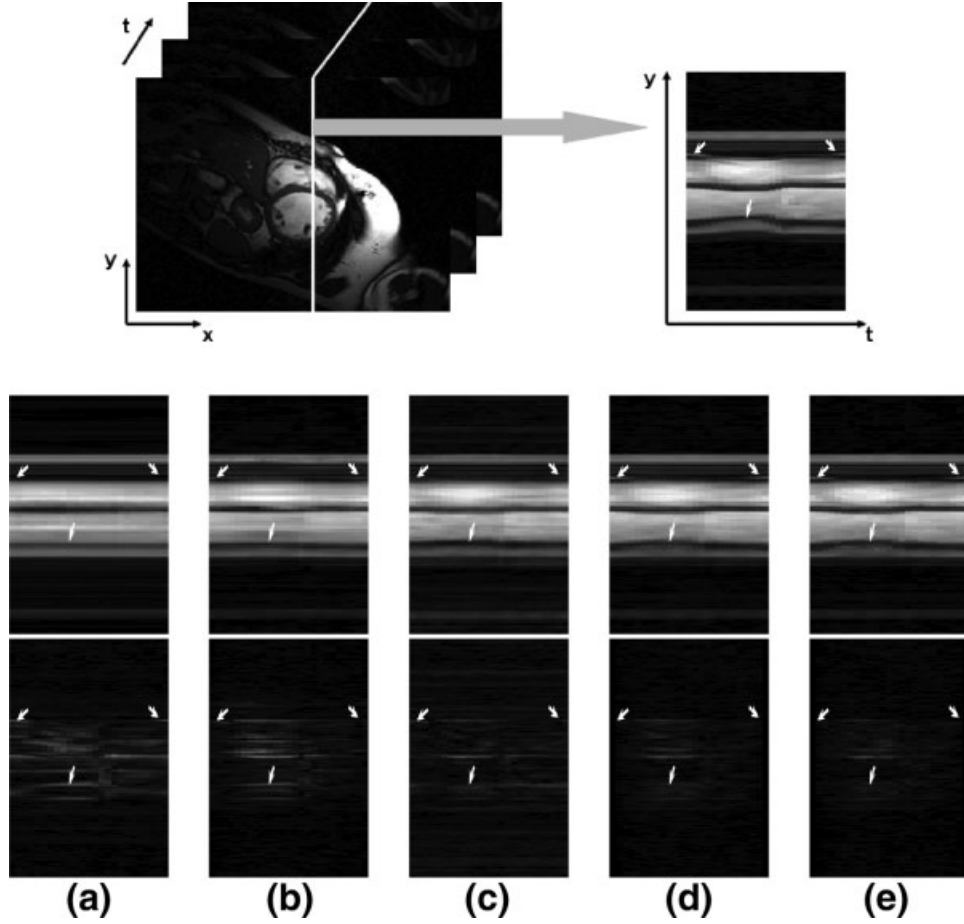


FIG. 6. Reconstructed y - t slices are shown to compare the temporal variation. On the top, the reference image from fully sampled k - t data is shown. Some significant movements of the heart are pointed with white arrows. The results of k - t BLAST, SPEAR, k - t FOCUSS with temporal average, k - t FOCUSS with 2-D RIGR and k - t FOCUSS with ME/MC are shown in (a), (b), (c), (d), and (e), respectively. In k - t FOCUSS with 2-D RIGR and k - t FOCUSS with ME/MC, the movement of heart is most clearly seen, and the difference signals are very small.

k - t FOCUSS algorithm consistently outperforms. For the higher acceleration factor, k - t BLAST/SENSE and SPEAR cannot effectively remove aliasing artifacts and these aliasing artifacts become very severe. In contrast, k - t FOCUSS methods effectively suppress aliasing artifacts and reconstruct much improved images compared to k - t BLAST/SENSE and SPEAR. The MSE plot also confirms quantitatively that k - t FOCUSS methods show improved performance. Especially, k - t FOCUSS with 2-D RIGR and ME/MC have the smallest MSE over all frames.

In Fig. 6, we illustrated the temporal variation of a slice from the cardiac volume. In this case, we used the second data set at a higher reduction factor of 11. Fully sampled 8 phase encoding lines in the low frequency region and 12 phase encodings for the high frequency region were sampled out of a total of 220 phase encodings. As a reference image, we illustrated the y - t image which is reconstructed from the fully sampled data set on the top of Fig. 6. Some heart movements are visible and are indicated with white arrows. However, in the k - t BLAST/SENSE reconstruction in Fig. 6a, there is no such movement due to the signal nulling problem. Recall that k - t BLAST/SENSE employs the lattice sampling pattern and initially subtracts temporal average in order to avoid energy concentration on the DC

term of the temporal Fourier transform. The subtraction of the temporal average forces the DC frequency zero, which is replicated in y - f domain due to the lattice sampling pattern. The number of the zero frequency replicas is determined by the acceleration factor. Even if k - t BLAST/SENSE unfolds aliasing of replicas on y - f space, the replicated frequencies initially set to zero cannot be recovered. As a consequence, no temporal variation is observed in (a). By resolving signal nulling problem, SPEAR in Fig. 6b shows some movements but this is still far from the reference movements. k - t FOCUSS with temporal average in Fig. 6c follows the movements much more clearly than above two methods. When k - t FOCUSS with 2-D RIGR or ME/MC in Fig. 6d,e are used, the reconstructed y - t image greatly follows the reference movements. The difference images much more clearly show the performance of each method. We have also plotted average pixel values within a 5 pixel by 5 pixel region of interest (ROI) along the temporal direction (see Fig. 7). The ROI was chosen at the area that has the most significant motion. We can clearly see that k - t FOCUSS with 2-D RIGR and ME/MC follows the true temporal variation much more accurately than any of the other methods while the other methods show temporal blurring compared to true variation. Note that k - t BLAST/SENSE can not follow

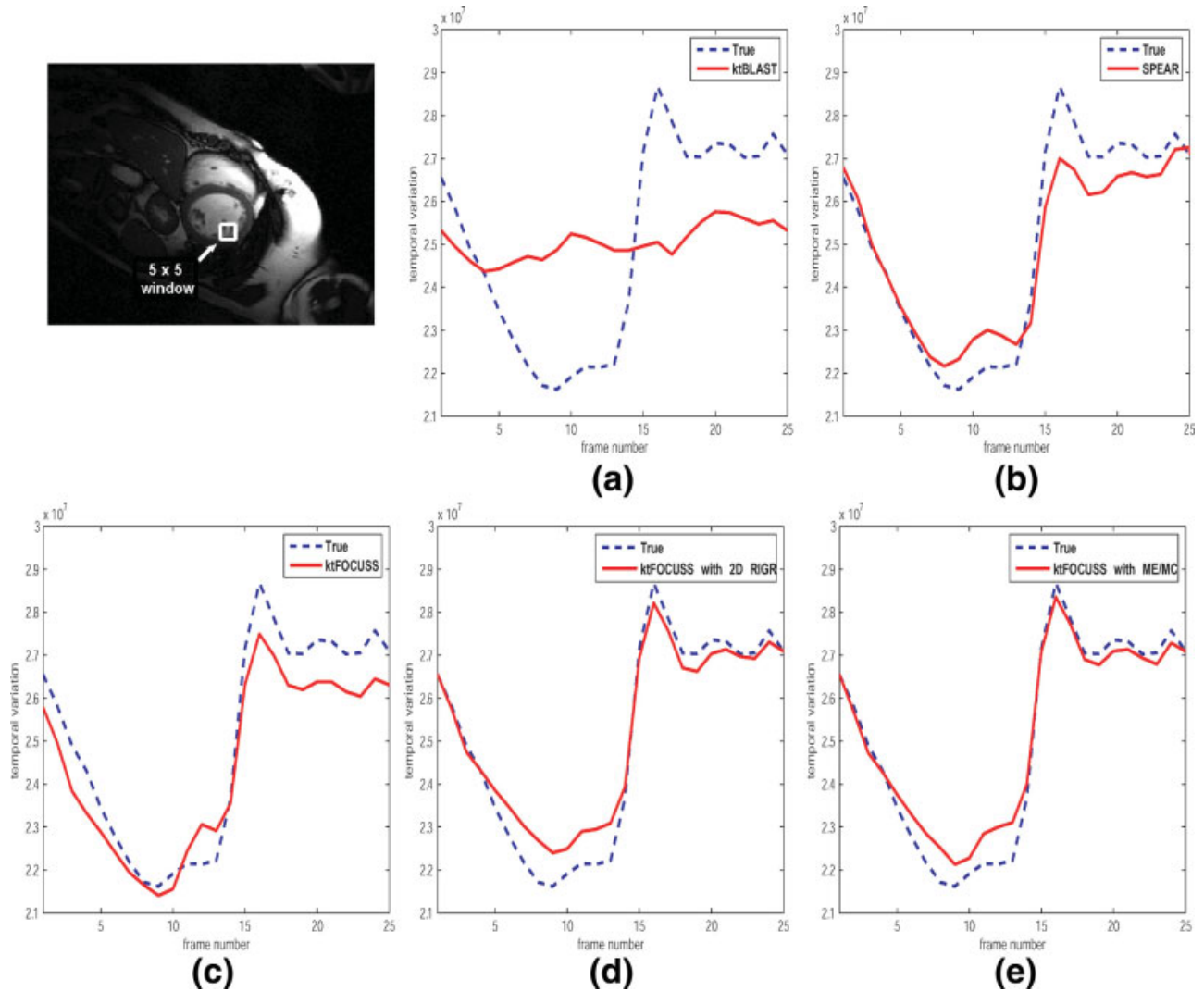


FIG. 7. The temporal variation of averaged signals in 5×5 pixels ROI for the case of (a) k-t BLAST, (b) SPEAR, (c) k-t FOCUSS with temporal average, (d) k-t FOCUSS with 2-D RIGR, and (e) k-t FOCUSS with ME/MC, respectively. In this experiment, the acceleration factor not including training data set was 16 and the total time frame number was 25. Because k-t BLAST initially subtracts the temporal average, the temporal DC frequency with zero values are also replicated in 16 times along the temporal frequencies out of the total 25 number of temporal frequencies. Consequently, more than half of original spectrum becomes zero. The zero value signal cannot be recovered through k-t BLAST, and results in the signal nulling problem. Consequently, (a) shows severely blurred temporal variation. Meanwhile, (d) and (e) follow the true temporal variation very closely. [Color figure can be viewed in the online issue, which is available at www.interscience.wiley.com.]

true variation at all because of severe signal nulling problem at high acceleration factor as explained above. We are aware that the original k-t BLAST/SENSE avoids such signal nulling problem by modifying the acquisition timing (9), which is, however, more complicated than the simple random sampling pattern used in k-t FOCUSS.

As discussed before, temporal Fourier transform works as a special case as a sparsifying transform and other transforms can also be used instead. To verify this, we applied a KLT (Karhunen-Loeve Transform) and a wavelet transform along the temporal direction and the spatial direction, respectively, as different choices of sparsifying transforms. For KLT, from the covariance matrix of the temporally varying images of intermediate k-t FOCUSS results, the KLT basis was obtained using eigen-decomposition. As a consequence, KLT can represent the temporally varying signal with only a few eigen-basis. Similarly, wavelet

transform can be considered as a sparsifying transform along the spatial direction. All these methods reconstruct better images than k-t BLAST and SPEAR. However, the improvement over the k-t FOCUSS with simple temporal Fourier transform was negligible, so we have not illustrated the reconstruction results.

In Vivo Experiments

Two cardiac phases representing diastole and systole reconstructed from the full data set are illustrated in Fig. 8b. These results were used as a reference for validation of the following k-t FOCUSS reconstruction from the accelerated data set. Figure 8c shows the direct inverse Fourier transform using the k-space data from the accelerated acquisition. Because of severe aliasing due to high acceleration, we cannot see any important features of the heart. Applying

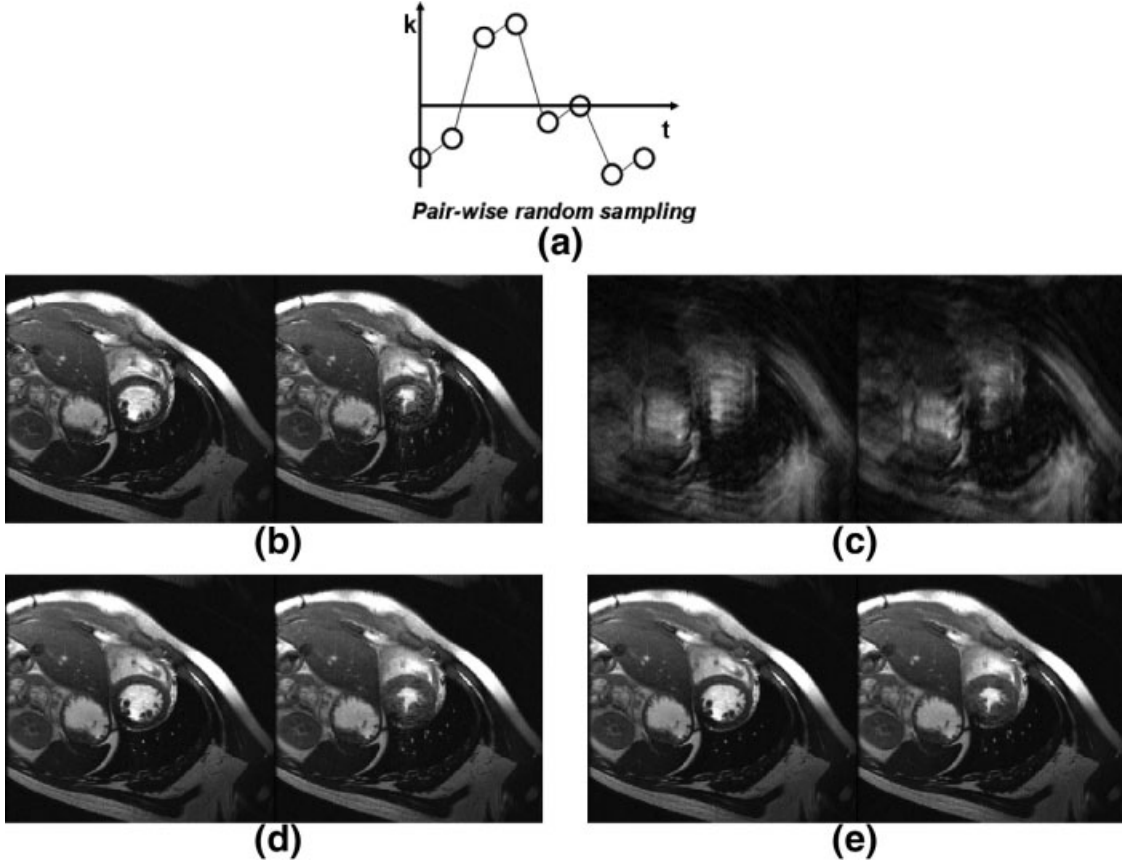


FIG. 8. *In vivo* experimental results. In order to reduce eddy current effects, pair-wise random sampling pattern as shown in (a) was employed at the acceleration factor of six. (b) shows reconstruction from fully sampled data. (c) shows the direct Fourier inversion reconstruction from $6\times$ accelerated acquisition, which shows serious aliasing artifacts. Applying k-t FOCUSS with 2-D RIGR and ME/MC, high resolution images were reconstructed as shown in (d) and (e), respectively. No aliasing artifacts were observed and diastole and systole of cardiac phase are clearly visible.

k-t FOCUSS with 2-D RIGR and ME/MC, we successfully reconstructed high resolution dynamic MR images without aliasing artifacts in Fig. 8d,e. Here, one of the frames from the full k-space acquisition was used as a reference frame for 2-D RIGR and ME/MC. Fig. 8d,e clearly show diastole and systole phases of the heart including the depiction of fine cardiac structure. Note that the full data acquisition required 24 heartbeats, whereas only 4 heartbeats were necessary for the accelerated data acquisition. We can expect the advantages of k-t FOCUSS to be more significant when applied to volumetric acquisitions.

To evaluate eddy current effects (25), we tested k-t FOCUSS with unpaired random phase encode ordering with the same acceleration factor of six. Results (not shown) exhibited very poor image quality.

DISCUSSION

Relation to k-t BLAST/SENSE and SPEAR

In Ref. 19, we showed that the conventional k-t BLAST/SENSE corresponds to the special case of our k-t FOCUSS with temporal average. In this article, we further extend the analysis and show that the SPEAR algorithm is also a special case of our k-t FOCUSS algorithm.

Recall that the equation for k-t BLAST/SENSE is given by

$$\rho = \bar{\rho} + \Theta \mathbf{F}^H (\mathbf{F} \Theta \mathbf{F}^H + \lambda \mathbf{I})^{-1} (\mathbf{v} - \mathbf{F} \bar{\rho}), \quad [24]$$

where \mathbf{F} denotes the 2-D Fourier transform and $\bar{\rho}$ is the temporal average of measurements, and Θ is a diagonal signal covariance matrix obtained from training or interleaved low frequency data. Note that the temporal DC term $\bar{\rho}$ is separately processed in Eq. [24]. Since most energy is concentrated on the DC frequency, signals at a higher temporal frequency band cannot be fully recovered unless the DC frequency is processed separately. However, the subtraction of the temporal average gives rise to a significant problem called signal nulling (13). This problem induces severe degradation for temporal resolution when the down-sampling ratio is high. To resolve this problem, SPEAR has been proposed recently using RIGR reconstruction instead of temporal average (13). The SPEAR update is exactly the same as that of k-t BLAST/SENSE except the initialization:

$$\rho = \rho_{RIGR} + \Theta \mathbf{F}^H (\mathbf{F} \Theta \mathbf{F}^H + \lambda \mathbf{I})^{-1} (\mathbf{v} - \mathbf{F} \rho_{RIGR}). \quad [25]$$

The only additional requirement for SPEAR is obtaining two reference frames at the beginning and the

end of dynamic encodings to incorporate the RIGR algorithm.

If we compare Eqs. [24] and [25] with our k-t FOCUSS update in Eq. [11], we can easily find that k-t BLAST/SENSE corresponds to the first iteration of k-t FOCUSS with temporal average, whereas SPEAR corresponds to the first iteration of k-t FOCUSS with RIGR. Note that k-t BLAST/SENSE and SPEAR use the lattice sampling pattern, which violates the incoherence of measurement in compressed sensing. Hence, these algorithms do not show improvement as the iteration number grows as discussed in Ref. 19. However, k-t FOCUSS is based on a random sampling pattern; hence, the results improve with the iteration as indicated by the theory.

Relation to UNFOLD and PARADIGM/PARADISE

The method called UNFOLD (UNaliasing by Fourier-encoding the Overlaps Using the temporal Dimension) (8) is another method for fast data acquisition using lattice sampling pattern. Theoretically, the optimal lattice design problem can be formulated as a spatio-temporal sampling problem in k-t space under the so-called time sequential sampling (TSS) constraint (26). Bresler et al. (27,28) proposed Patient-Adaptive Reconstruction and Acquisition Dynamic Imaging Method (PARADIGM) that achieves a high temporal and spatial resolution with a multifold reduction using the optimal TSS pattern calculated on the fly. A generalization of TSS for the phase array coil data acquisition called Patient-Adaptive Reconstruction and Acquisition Dynamic Imaging with Sensitivity Encoding (PARADISE) has been recently proposed by Sharif et al. (29,30). The maximum achievable acceleration factor can be up to the parallel imaging acceleration factor multiplied by that of the optimized time sequential sampling.

In theory, if the signal is band-limited and the exact support can be estimated, PARADISE and PARADIGM are optimal in the sense that they provide the minimal distortion in the reconstructed image by adaptively estimating the coefficients. More specifically, the reconstruction error from such adaptive estimation is given as follows (15):

$$\|\rho - \rho_{adapt,M}^*\|_2 \lesssim M^{-r}$$

where $\rho_{adapt,M}^*$ denotes the adaptive estimate from M measurements and the decay rate r depends on the signal smoothness. However, in many applications, the signal support is not band-limited and is difficult to estimate in real time. In this case, a compressed sensing approach like k-t FOCUSS using random sampling pattern is a perfect fit since the unknown sparse signal can be simultaneously estimated during the l_1 minimization process and no additional steps are required for support estimation. However, a blind use of a compressed sensing approach like k-t FOCUSS requires a little caution. Donoho et al. (15) showed that the error decay rate for the compressed sensing approach is given by

$$\|\rho - \rho_{cs,M}^*\|_2 \lesssim (M/\log N)^{-r}$$

where $\rho_{cs,M}^*$ denotes the compressed sensing estimate using M samples, and N denotes the total length of the unknown signal. This implies that in order to achieve similar reconstruction error as in adaptive estimation, compressed sensing reconstruction must pay $\log N$ penalties in total number of k-t samples. Still, if the signal is sparse in some basis, the resultant k-t sample number is much smaller than the Nyquist rate even with the $\log N$ penalty, hence validating the advantage of k-t FOCUSS. Furthermore, any type of temporal transform can be used for k-t FOCUSS as long as it can effectively sparsify the unknown signal, whereas the aforementioned lattice sampling approaches usually require temporal Fourier transforms. Therefore, we believe that k-t FOCUSS can find many important applications in dynamic MR imaging applications.

2-D RIGR vs. ME/MC

In this article, we have compared the k-t FOCUSS with 2-D RIGR and ME/MC. The results indicate that k-t FOCUSS with ME/MC outperforms k-t FOCUSS with 2-D RIGR. Then, one may wonder why we are interested in 2-D RIGR prediction at all. The main reason concerns computational complexity. 2-D RIGR exploits the temporal redundancies in k-space whereas ME/MC decorrelates the temporal correlation using motion estimation in the spatial domain. It turns out that the motion estimation step is the most time-consuming part in video coding (23). Furthermore, k-t FOCUSS with ME/MC requires additional application of k-t FOCUSS for motion estimation. Though the final reconstruction quality of k-t FOCUSS with 2-D RIGR is not as good as k-t FOCUSS with ME/MC, the computational complexity is very small and can be implemented in real time. However, it is important to note that when the k-t space trajectory is non-cartesian, ME/MC can still be applied, whereas the RIGR algorithm only works for cartesian theory. Therefore, users should make a judicious decision on which prediction scheme should be used.

Reference Frames

Even though one or two reference frames are used for the prediction step using 2-D RIGR and ME/MC, they are not mandatory for k-t FOCUSS. Specifically, even if no reference frame is available, at least one reference frame can be generated using temporal average image of k-t measurements. Figure 9 clearly shows that 2-D RIGR and ME/MC can be very effectively used even if no reference frame is available. Here, 2-D RIGR and ME/MC were performed using temporal average as a reference frame. Compared to k-t FOCUSS which uses just temporal average as a prediction (a), k-t FOCUSS with 2-D RIGR (b) and ME/MC (c) clearly reduce aliasing artifacts for the same down sampled data even without the reference frames. The MSE plot (d) also confirms this quantitatively.

Actually, the advantage of using additional one or two fully sampled reference frame is to minimize the error propagation in the 2-D RIGR and ME/MC prediction especially at the high acceleration factor. Furthermore, there are many practical dynamic MR applications where we can

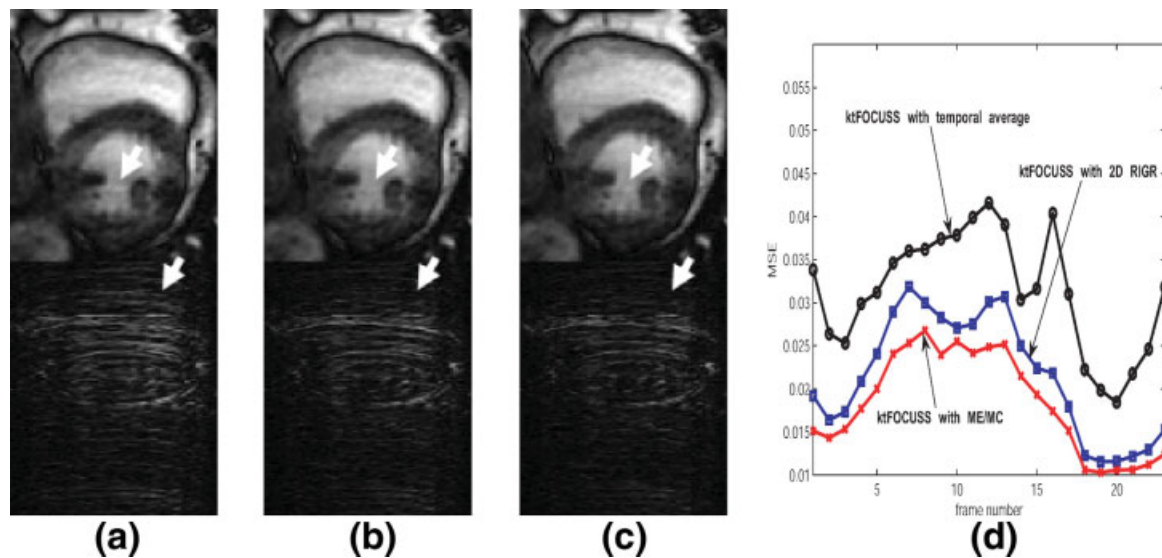


FIG. 9. When two fully sampled reference frames are not available, 2-D RIGR and ME/MC can still work using temporal average as a reference frame. (a) k-t FOCUS with temporal average, (b) k-t FOCUS with 2-D RIGR, and (c) k-t FOCUS with ME/MC. (d) frame-by-frame MSE plots. See white arrows. The artifacts seen in (a) disappear in (b) and (c). [Color figure can be viewed in the online issue, which is available at www.interscience.wiley.com.]

easily obtain fully sampled reference frames. For example, in fMRI applications, we can easily obtain the fully sampled reference frame during the resting phase of the paradigm. Other applications include perfusion imaging, contrast enhanced angiography, diffusion tensor imaging (DTI), and etc, where we can control the initiation of the activation.

Extension to fMRI

Throughout the article, our new algorithm has been applied to reconstruct high spatio-temporal resolution from very limited data samples in dynamic cardiac MR imaging. However, another important application that requires very high spatio-temporal resolution is functional MR imaging (fMRI). Recall that fMRI is a technique to monitor brain hemodynamics for specific stimulus, behaviors, or mental status of a subject. Usually, fMRI data are scanned with very fast imaging sequence such as EPI. For the matrix size of $64 \text{ pixels} \times 64 \text{ pixels}$, two or three second temporal resolution can be achieved for covering whole brain using EPI sequence. However, the highly accelerated acquisition is often required for the extensive analysis of cognitive fMRI study using higher resolution EPI images. For this application, k-t FOCUS can be employed. In Ref. 19, we briefly demonstrated the feasibility of k-t FOCUS for the accelerated acquisition of fMRI data. Using improved k-t FOCUS with new prediction and residual encoding, we can expect that more accurate reconstruction may be feasible. However, extensive statistical analysis must be performed for a wide acceptance of this technique in fMRI.

CONCLUSION

This article described a generalization of k-t FOCUS that is optimal from the compressed sensing perspective. k-t

FOUSS reconstruction consists of two terms; one from prediction, and the other from residual encoding. Then, the optimal k-t FOCUS design problem becomes optimal sample allocation between the prediction and residual encoding steps. We proposed two prediction schemes based on a novel 2-D RIGR and ME/MC. Both approaches try to decorrelate the temporal correlation between the frames using estimation in the Fourier or spatial domain, respectively. In order to further sparsify the residual signal, k-t FOCUS allows various temporal transforms optimized for specific dynamic MR applications. We also showed that conventional k-t BLAST/SENSE and SPEAR correspond to the special case of our k-t FOCUS. Experimental results confirmed that high spatio-temporal resolution can be achieved using k-t FOCUS even from severely undersampled k-t measurements.

ACKNOWLEDGMENTS

The authors would like to thank Dr. Joon Young Jeong and Prof. Zang-Hee Zho at Gacheon Neuroscience Research Institute (NRI) at Incheon, Korea, for various assistance.

REFERENCES

1. Carr HY. Steady-state free precession in nuclear magnetic resonance. *Phys Rev* 1958;112:1693–1701.
2. Plein S, Bloomer TN, Ridgway JP, Jones TR, Bainbridge GJ, Sivanathan MU. Steady-state free precession magnetic resonance imaging of the heart: Comparison with segmented k-space gradient-echo imaging. *J Magn Reson Imaging* 2001;14:230–236.
3. Lee VS. Cardiovascular MRI: physical principles to practical protocols. Philadelphia: Lippincott Williams & Wilkins; 2005.
4. Sodickwon DK, Manning WJ. Simultaneous acquisition of spatial harmonics (SMASH): Fast imaging with radiofrequency coil arrays. *Magn Reson Med* 1997;38:591–603.
5. Griswold MA, Jakob PM, Heidemann RM, Nittka M, Jellus V, Wang J, Kiefer B, Haase A. Generalized autocalibrating partially parallel acquisitions (GRAPPA). *Magn Reson Med* 2002;47:1202–1210.

6. Griswold MA, Jakob PM, Nittka M, Goldfarb JW, Haase A. Partially parallel imaging with localized sensitivities (PILS). *Magn Reson Med* 2000;44:602–609.
7. Pruessmann KP, Weigher M, Scheidegger MB, Boesiger P. SENSE: Sensitivity encoding for fast MRI. *Magn Reson Med* 1999;42:952–962.
8. Madore B, Glover GH, Pelc NJ. Unaliasing by Fourier-encoding the overlaps using the temporal dimension (UNFOLD), applied to cardiac imaging and fMRI. *Magn Reson Med* 1999;42:813–828.
9. Jeffrey Tsao, Boesiger P, Pruessmann KP. k-t BLAST and k-t SENSE: Dynamic MRI with high frame rate exploiting spatiotemporal correlations. *Magn Reson Med* 2003;50:1031–1042.
10. Kozerke S, Tsao J, Reza Razavi, Boesiger P. Accelerating cardiac cine 3D imaging using k-t BLAST. *Magn Reson Med* 2004;52:19–26.
11. Tsao J, Kozerke S, Boesiger P, Pruessmann KP. Optimizing spatiotemporal sampling for k-t BLAST and k-t SENSE: Application to high-resolution real-time cardiac steady-state free precession. *Magn Reson Med* 2005;53:1372–1382.
12. Hansen MS, Kozerke S, Pruessmann KP, Boesiger P, Pedersen EM, Tsao J. On the influence of training data quality in k-t BLAST reconstruction. *Magn Reson Med* 2004;52:1175–1183.
13. Xu D, King KF, Liang Z-P. Improving k-t SENSE by Adaptive Regularization. *Magn Reson Med* 2007;57:918–930.
14. Liang Z-P, Lauterbur PC. An efficient method for dynamic magnetic resonance imaging. *IEEE Trans Med Imaging* 1994;13:677–686.
15. Donoho DL. Compressed sensing. *IEEE Trans on Inform Theory* 2006;52:1289–1306.
16. Candes E, Romberg J, Tao T. Robust uncertainty principles: Exact signal reconstruction from highly incomplete frequency information. *IEEE Trans Info Theory* 2006;52:489–509.
17. Lustig M, Santos JM, Donoho DL, Pauly JM. k-t SPARSE: High frame rate dynamic MRI exploiting spatio-temporal sparsity. In *Proceedings of ISMRM, Seattle, WA, April 2006*.
18. Lustig M, Donoho DL, Pauly JM. Sparse MRI: The application of compressed sensing for rapid MR imaging. *Magn Reson Med* 2007;58:1182–1195.
19. Jung H, Ye JC, Kim EY. Improved k-t BLAST and k-t SENSE using FOCUSS. *Phys Med Biol* 2007;52:3201–3226.
20. Gorodnitsky IF, George JS, Rao BD. Neuromagnetic source imaging with FOCUSS: A recursive weighted minimum norm algorithm. *Electroencephalogr Clin Neurophysiol* 1995;95:231–251.
21. Gorodnitsky IF, Rao BD. Sparse signal reconstruction from limited data using FOCUSS: Re-weighted minimum norm algorithm. *IEEE Trans Signal Processing* 1997;45:600–616.
22. Kreuz-Delgado K, Murray JF, Rao BD, Engan K, Lee TW, Sejnowski TJ. Dictionary learning algorithms for sparse representation. *Neural Comput* 2003;15:349–396.
23. Gall DL. MPEG: A video compression standard for multimedia applications. *Commun ACM* 1991;34:46–58.
24. Wang Y, Ostermann J, Zhang Y-Q. *Video processing and communications*. New Jersey: Prentice Hall; 2002. pp. 153–154.
25. Bieri O, Markl M, Scheffler K. Analysis and compensation of eddy currents in balanced SSFP. *Magn Reson Med* 2005;54:129–137.
26. Aggarwal N, Zhao Q, Bresler Y. Spatio-temporal modeling and minimum redundancy adaptive acquisition in dynamic MRI. *Proceedings of IEEE ISBI 2002*;730–740.
27. Zhao Q, Aggarwal N, Bresler Y. Dynamic imaging of time-varying objects. *Proceedings of ISMRM, 2001*, p. 1776.
28. Bresler Y. Fast acquisition and sampling in MRI: Introduction to time-sequential sampling of spatio-temporal signals. In *Proceedings of IEEE ISBI, 2002*, pp. 713–716.
29. Sharif B, Bresler Y. Optimal multi-channel time-sequential acquisition in dynamic MRI with parallel coils. *Proceedings of IEEE ISBI, 2006*, pp. 45–48.
30. Sharif B, Bresler Y. Adaptive real-time cardiac MRI using PARADISE: Validation by the physiologically improved NCAT phantom. In *Proceedings of IEEE ISBI, April 2007*.